Magnetic Characterization of the Altermagnetic Material CrSb

Gabriel Textorius

under the supervision of
Erik Walterson

School Year 25/26

January 31, 2026

Abstract

Altermagnets is a new type of magnetic material which combines some properties of ferromagnets and antiferromagnets. In this project, the magnetic response of the CrSb sample in the x, y and z directions as a function of temperature and magnetic field was measured. By measuring the difference in susceptibility along different axes, the degree of anisotropy was determined. The difference in susceptibility depending on whether Zero Field Cooled or Field Cooled measurements were done also revealed more about the material. By fitting the temperature dependence of susceptibility to a modified Curie-Weiss Law, the Curie constant was extracted which later allowed the finding of the magnetic moment of the involved ions in the material. This in turn was compared to the magnitude of the moments of the ions when viewed in isolation. The altermagnetic material assessed was a CrSb crystal. The results show clear magnetic anisotropy with the b-axis being the preferred magnetization axis. ZFC-FC splitting only appeared along the a-axis with no splitting on the b-axis or c-axis. The difference in magnetic moments between the measurement and the one predicted by theory suggests that itinerant magnetism is a significant contributing factor to the susceptibility of CrSb. The M vs. H measurements showed no strong signs of hysteresis. More sophisticated models need to be used in future experiments to further characterize CrSb.

Acknowledgements

Contents

References   **25**

1   Introduction

The existence of a new type of magnetism, coined altermagnetism, was first experimentally demonstrated in 2024 [1]. Combining two different states of permanent magnetism, altermagnetism shows promise for having use within the evolving field of spintronics, potentially aiding in creating new and more efficient types of devices. However, due to the recency of their discovery, more experiments need to be made in order to understand the subtleties of how altermagnets work, which materials are the best candidates for creating altermagnets, and how these materials are best used [2]. This can be done by measuring the magnetic susceptibility of the magnet, which quantifies how much the magnet contributes to an externally applied magnetic field [3].

1.1   CGS-system

One important thing to note is that the field of magnetism within solid state physics usually uses the CGS measurement system. Unlike the SI-system, where the units for mass, time, and length are kilogram, seconds and meter, CGS uses the units grams, seconds, and centimeters. Additionally, the units for many concepts in magnetism are different. Most importantly for this report, following the conventions of the field, magnetic moment will be measured in emu[1] and magnetic field strength in Oe.

1.2   Crystal Structures, Reciprocal Space and Fermi Levels

Crystal structures are defined by their periodicity. They are built up from a basis which is repeated over the entire crystal structure, providing some symmetries [5]. This periodicity means that describing one smaller part of the crystal can be extended to almost the entire crystal. By studying the electrons within the crystal, one can see that some of them are localised, meaning they generally exist near their associated atomic nuclei, while other electrons are delocalised, meaning the have a greater ability to move throughout the

---

[1]Calling emu a unit is slightly misleading as there are some subtleties to the situation that can not be covered in this report. For more information regarding the history of CGS vs. SI in magnetism and some conversions, see [4].

crystal structure. The crystal structure exists within a 3-dimensional real space described by the x, y and z axis. By taking the Fourier Transform of the space, the mathematical reciprocal space of the crystal structure is defined, also known as the momentum-space, or k-space for short [6]. In the k-space, the units are in reciprocal length and each position in the k-space represents a wavevector **k**. A wavevector has the magnitude of the wavenumber which is in turn equal to $|k| = \frac{2\pi}{\lambda}$, where λ is the wavelength. The direction of a wavevector is along the direction in which the wave propagates [5]. Using the k-space for describing how electrons behave within a crystal structure is useful as the wavevector is proportional to the momentum of the electron, which is used to describe some of its properties [7]. Therefore, this report will use the k-space for explanations describing how magnetism and altermagnets work.

One property of the k-space is that one may measure how much energy is required for an electron to exist at a certain point of the k-space. One way to do this is the following: The binding energy for an electron is given by the formula

$$E_b = \frac{p^2}{2m} \tag{1}$$

where E_b is the binding energy, p the momentum of the particle and m the mass of the particle [8]. This equation may be rewritten through the formula $p = \hbar k$ where k is the wavevector of the particle. This is because quantum mechanics, specifically the de Broglie relation [7], tells us that the momentum of a particle is proportional to its wavevector, with the constant of proportionality being $\hbar$, the reduced Planck's constant. This means that Equation (1) may be rewritten as

$$E_b = \frac{\hbar^2 k^2}{2m}. \tag{2}$$

This in turn means that for any point in the k-space, the binding energy for an electron may be found. If one then moves through k-space such that the wavevector changes linearly, the binding energy will change quadratically. In other words, the shape of the
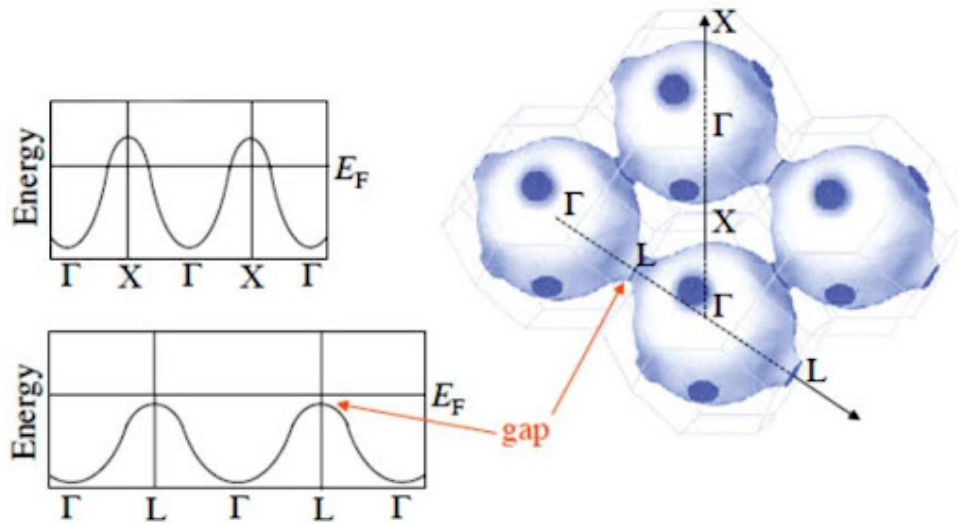
Figure 1: (Left) Graph of the band structure where the y-axis shows the energy and the x-axis different positions in k-space, here denoted by different Greek letters. (Right) Visualisation of the Fermi surface for a compund. Image courtesy of Prof. Yasmine Sassa.

energy as a function of position in k-space can be expected to be parabolic.

One important energy level to keep track of in the k-space is the Fermi Level which, among other things, denotes the maximum energy state for an electron at the temperature 0 K [9]. To visualize the Fermi Level, a 3D model of the k-space can include a surface which denotes the location in the k-space where the Fermi level resides. These surfaces are also known as Fermi surfaces. Visualisations of the different energy levels within the k-space in the form of band structure graphs and an example of a Fermi surface is found in Figure 1. One can also note the parabolic shape of the band structures when below the Fermi level, before it changes direction above the Fermi level. One interesting aspect of the energy levels within the k-space is that, in some materials, different spin orientations have different energy levels required in the same position within the k-space.

1.3   Ferromagnetism

There are various types of magnetism. The first, and most well known, is ferromagnetism. In a material featuring ferromagnetism, all spins within a magnetic domain of the material are aligned in parallel within the direct space, as seen in Figure 3a. This alignment is said to be spontaneous, meaning an external magnetic field does not need to be applied for this

alignment to happen [3]. The spontaneous alignment causes a spin-splitting within the materials, with one orientation of electron spin being more energetically favourable. This is seen in k-space where the same location in the k-space has two different energy levels, one for spin up, the other for spin down, also seen in Figure 3a [10]. The direction of spin which is favoured is the same within the entire magnetic domain. There can be different causes for this spin-splitting within different materials. If magnetic domains are aligned in the same direction, a macroscopic magnetic field is generated. This is what causes everyday permanent magnets to function. This magnetic ordering can, however, be disrupted if the system contains enough thermal energy. The specific temperature where a ferromagnet loses its spontaneous magnetic ordering is called the Curie temperature. Ferromagnets also possess many other useful properties not directly related to their generated macroscopic magnetic fields. The generated field can be disrupted if one applies a magnetic field in the opposite direction. If one then sweeps the field from strong in one direction before weakening and reaching zero before increasing in the opposite direction, one can see how the magnetic field contributed from the ferromagnet suddenly disappears and contributes in the other direction. The resulting graph thus exhibits a loop, which is called a hysteresis loop. [3]

1.4   Antiferromagnetism

A different type of magnetism is antiferromagnetism. Unlike ferromagnetism, where spins are aligned to constructively give rise to a larger magnetic field, antiferromagnetism entails the spins within a material being ordered in such a way as to make all spins cancel each other. Antiferromagnets do not have any spin splitting. Therefore, one spin orientation is not energetically more or less costly than the other. Looking at the momentum space, one can see that all positions within it have the same energy required for both spin directions. This can all be seen in Figure 3b. The antiferromagnetic order within the material only exists below the Néel temperature due to the thermal excitations of atoms disrupting the magnetic order above the Néel temperature. The Néel temperature is analogous to the Curie temperature for ferromagnets. [3]

1.5   Other Magnetic Effects

Two other types of magnetism are paramagnetism and diamagnetism. Unlike ferro- and antiferromagnetism, para- and diamagnetism are not formed spontaneously. Paramagnetism only occurs when a material is exposed to an external magnetic field which induces a weak field within the material in the same direction as the external field. Diamagnetism is similar, with the main difference being that the induced field is in the opposite direction of the applied external field, and the material is thus repelled by the field. The diamagnetic contribution is also often far smaller than any paramagnetic contribution [3]. Paramagnetic and diamagnetic interactions can be found in many materials, even non magnetic ones such as water. It is through the diamagnetic contribution of water that frogs have been made to levitate in extremely strong magnetic fields, as seen in Figure 2 [11].

1.6   Altermagnetism

Despite their names and properties implying mutual exclusivity, ferromagnetism and antiferromagnetism can in some sense be combined [2]. The phenomenon of a combination of ferro- and anti-ferromagnetism is found within the newly discovered altermagnets [10]. Despite sharing the antiferromagnetic properties of no macroscopic magnetic field, resistance to external disturbance and the cancellation of magnetic moments, altermagnets also display properties commonly associated with ferromagnets, such as time-reversal asymmetry and spin-polarization in the band structure [2]. The k-space of an altermagnet is therefore characterised by having different spin orientations being the least energetically taxing at different points of the momentum space, as seen in Figure 3c. This means that altermagnets show promise as a material to be used in spintronic devices due to possessing useful ferromagnetic properties, without sharing the associated instability and tendency to affect nearby materials with stray fields [12]. Another promising quality of altermagnets is the large quantity of materials which may form altermagnets as well as their relative ease of access, not being far too exotic materials. One such candidate is chromium antimonide (CrSb) which has already shown itself to possess altermagnetic properties [13].

Figure 2: Image of frog levitating due to the diamagnetic contribution of water in strong magnetic fields. Photo taken by Andre Geim.
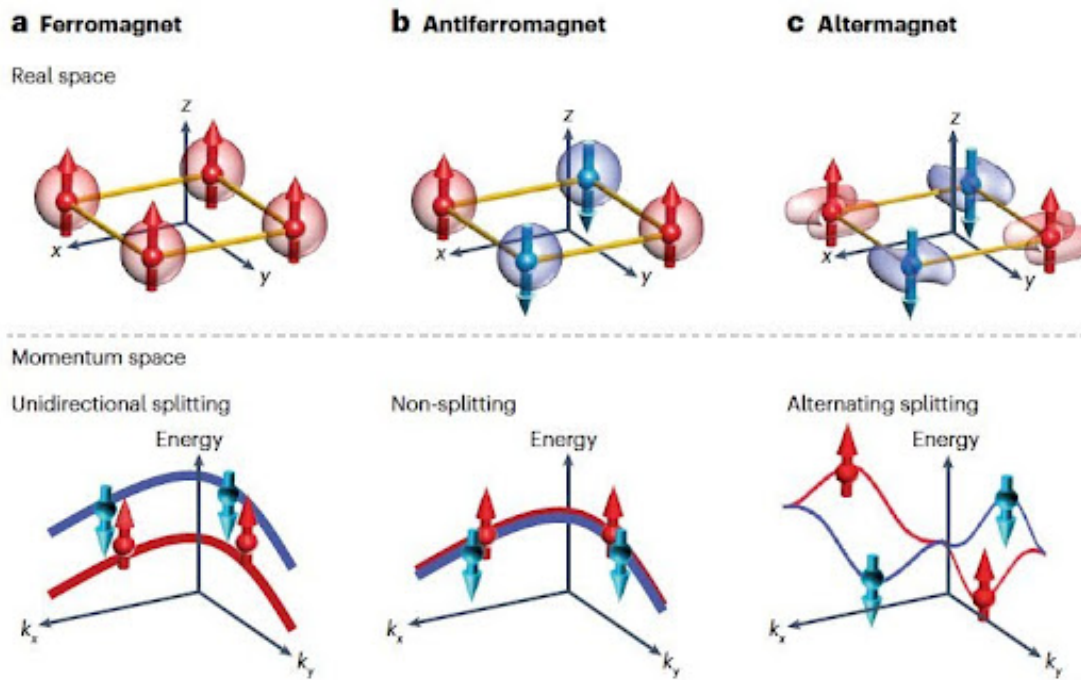
Figure 3: Top images showcase spin direction in real space for ferromagnets, antiferromagnets and altermagnets. The x-, y-, and z-axes represent real space. The images below show the band splitting, or lack thereof, for each type of magnet in the k-space (also known as momentum space) [10]. Here, the x- and y-axes show position in k-space, while the z-axes show the energy. The red and blue bands show the difference in energy for spin up and spin down.

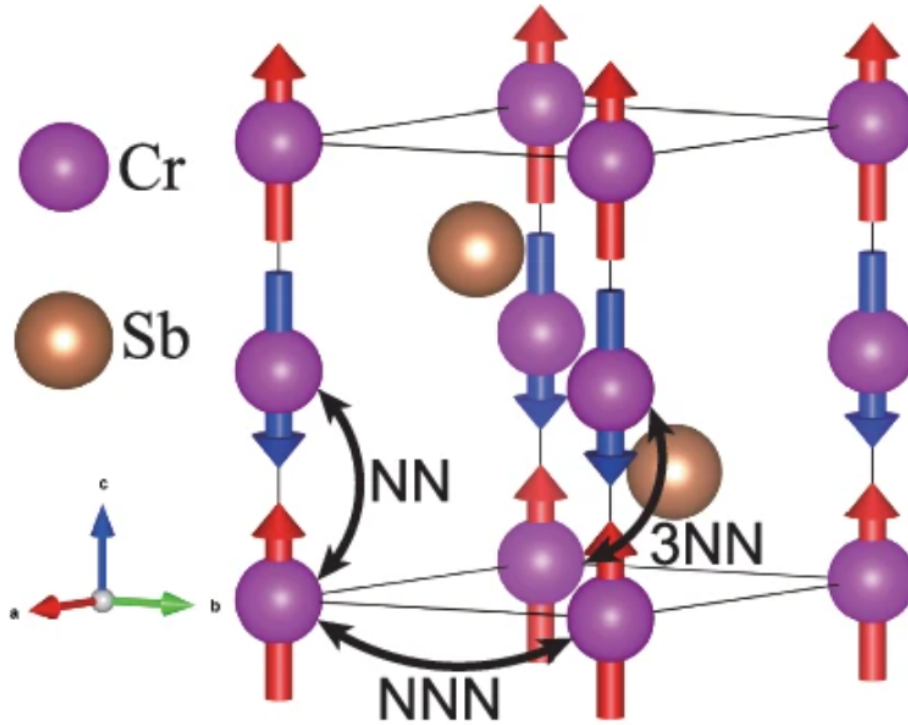Figure 4: Crystal structure of CrSb with the spins of the Cr atoms marked. Image from [14].

1.7   Chromium Antimonide

CrSb has been studied for its altermagnetic properties, which can be seen through its spin-splitting near the Fermi Level [14]. It has also been found that the Néel temperature of CrSb is quite high at 712 K meaning that the material does not need to be cooled below room temperature in order to retain its antiferromagnetic properties [13]. CrSb crystals have been shown to exhibit a NiAs type crystal structure, as seen in Figure 4 [14]. Previous measurements of the magnetic susceptibility of CrSb crystals have been made, but the magnetic anisotropy of the material has not been as extensively studied [13].

1.8   Localized vs. Itinerant Magnetism

Magnetism from a material can have its source at the level of localized electrons or through special interactions between delocalized electrons. On the localized level, magnetization appears due to these localized electrons, meaning those more or less fixed around a specific atom or ion, being ordered in a specific direction. Itinerant magnetism, involving electron

interactions, use the delocalized electrons in a material's collective electron bands. Two examples of itinerant magnetism are Pauli paramagnetism and Landau diamagnetism, both of which concern themselves with the spin direction of conduction band electrons. [3]

1.9   Magnetic Anisotropy

For certain magnetic materials, the orientation of the sample has an effect on the magnetization. This is due to the anisotropic materials having crystal structures that make some directions of magnetic moments require less energy. The magnetization of such materials is thus dependent on the direction in which the magnetic field is applied. Finding which direction is easier to magnetize is important for understanding how to use the material in applications most efficiently. [3]

1.10   Magnetic Moments

A magnetic moment is used when referencing how much individual particles contribute to a magnetic field. This is usually measured in Bohr magnetons, μ_B, which is defined by

$$\mu_B = \frac{e\hbar}{2m_e}.$$ (3)

Here, e is the elementary charge, $\hbar$ is the reduced Planck's constant, and m_e is the electron mass. Note that it is convention within this field to use CGS-units instead of SI-units. When calculating the magnetic moment of particles, the effective magnetic moment is used. The effective magnetic moment is related to the Curie constant through the equation:

$$C = \frac{N_A \mu_{\text{eff}}^2}{3k_B}$$ (4)

where C is the Curie constant, N_A is Avogadro's number, μ_{eff} is the effective magnetic moment and k_B is the Boltzmann constant. By rearranging Equation (4) the form

$$\mu_{\text{eff}} = \sqrt{\frac{3k_B C}{N_A}}.$$ (5)

is found which means that the effective moment can be found if the Curie constant is known.

The method above can be used for magnetic crystals, but a different formula is used when considering free ions without the interactions between particles. The formula follows

$$\mu_{\text{eff}} = \sqrt{n(n+2)}\mu_B \tag{6}$$

where n is the number of unpaired electrons.

1.11   Curie-Weiss Behaviour

One common method for analysing the behaviour and properties of magnetic materials is studying if and when it follows Curie-Weiss Behaviour. The Curie-Weiss law states that the magnetization of a material in a unchanging external magnetic field is inversely proportional to the temperature. Specifically, the Curie-Weiss law states that

$$\chi = \frac{C}{T - \theta_{CW}} \tag{7}$$

where C is the Curie constant, specific to the material, T is the temperature, θ_{CW} is the Curie-Weiss temperature and χ is the magnetic susceptibility of the material [3]. The susceptibility, in turn, governs the magnetization of the sample according to the relation

$$M = \chi H \tag{8}$$

where M is the magnetization and H the external magnetic field. The Curie-Weiss law is expected to hold when the material is in a paramagnetic state, meaning that the temperature is high enough to disrupt the magnetic ordering in the material. To find whether the Curie-Weiss law is the main factor for magnetization, it is often useful to plot the inverse of χ as a function of temperature and then observe whether a linear relation is

found. Taking the inverse of χ, one obtains the equation

$$\chi^{-1} = \frac{T}{C} - \frac{\theta_{CW}}{C} \tag{9}$$

is found. The curve, if it follows Curie-Weiss behaviour, will then be linear with slope of $1/C$ and y-intercept of $-\theta_{CW}/C$ if the line is extended to $T = 0\ K$.

The Curie-Weiss law can still be used on materials with more than just a paramagnetic contribution by adding some terms as follows:

$$\chi = \frac{C}{T - \theta_{CW}} + \chi_0 + aT. \tag{10}$$

The χ_0 term represents a temperature independent contribution to the susceptibility, while the aT term represents a susceptibility which is linearly dependent on the temperature. With the added complexity of the equation, simply taking the inverse and finding a linear fit is no longer feasible, so more advanced line fitting tools need to be used to find all four unknown parameters.

1.12 Aim of This Study

This report aims to measure the magnetic susceptibility of CrSb as a function of temperature and magnetic field strength and analyse how well it follows the Curie-Weiss law, or if a modified version of it needs to be used. The study also aims to analyse CrSb's anisotropic properties and investigate if any ZFC-FC splitting occurs within the material.

2   Method

All measurements were made using a Physical Property Measurement System (PPMS) which allows one to measure the magnetization of a sample both as a function of temperature and as a function of the applied external magnetic field. The PPMS contains a sample holder which may oscillate up and down at a frequency of 40 Hz with an amplitude

of 1-3 mm. This oscillation causes a change in the magnetic field generated by the sample, meaning a voltage is induced in a nearby detection coil. The PPMS also contains coils used for generating magnetic fields that can reach large magnitudes [15].

2.1 Magnetization vs. Temperature

The sample was cut into a block of dimensions $0.15 \times 0.08 \times 0.01 \text{cm}^3$. It was then attached to the sample holder, using varnish, at an offset of as near 35 mm as possible. The sample holder was put into the PPMS and an automatic centering routine was performed. A macro was created which instructed the PPMS to first lower its temperature to 5 K without any magnetic field and only afterwards applying a 1 T magnetic field in order to measure the Zero Field Cooled (ZFC) properties. The temperature was then slowly raised while measurements of the magnetization were performed until the temperature reached 300 K. After reaching 300 K, the temperature was dropped to 5 K again, this time with the magnetic field active during the cooling in order to perform Field Cooled (FC) measurements. After reaching 5 K, the temperature was slowly raised back to 300 K while measurements were made and the data saved. After the first experiment, the experiment was repetead, but with the sample rotated by 90° to measure the anisotropic effects. The first position was denoted the a-axis and the second was denoted the b-axis. A third experiment was done with the sample position changed to have it perpendicular to the front of the sample in experiments one and two, as seen in Figure 6.

2.2 Magnetization vs. Magnetic Field

The PPMS was mounted with a thin sample of CrSb with dimensions $0.15 \times 0.08 \times 0.01 \text{cm}^3$. The PPMS was then activated at a temperature of 300 K and a magnetic field of 9 T. The magnetic field was then gradually lowered while the resulting magnetization of the sample was recorded. The magnetic field was lowered to 0 Tesla before being increased again, but in the opposite direction, which can also be thought of as a negative field. This field was increased/decreased all the way to -9 T, before once again changing direction and gradually reaching + 9 T again. The same procedure was repeated for the temperatures
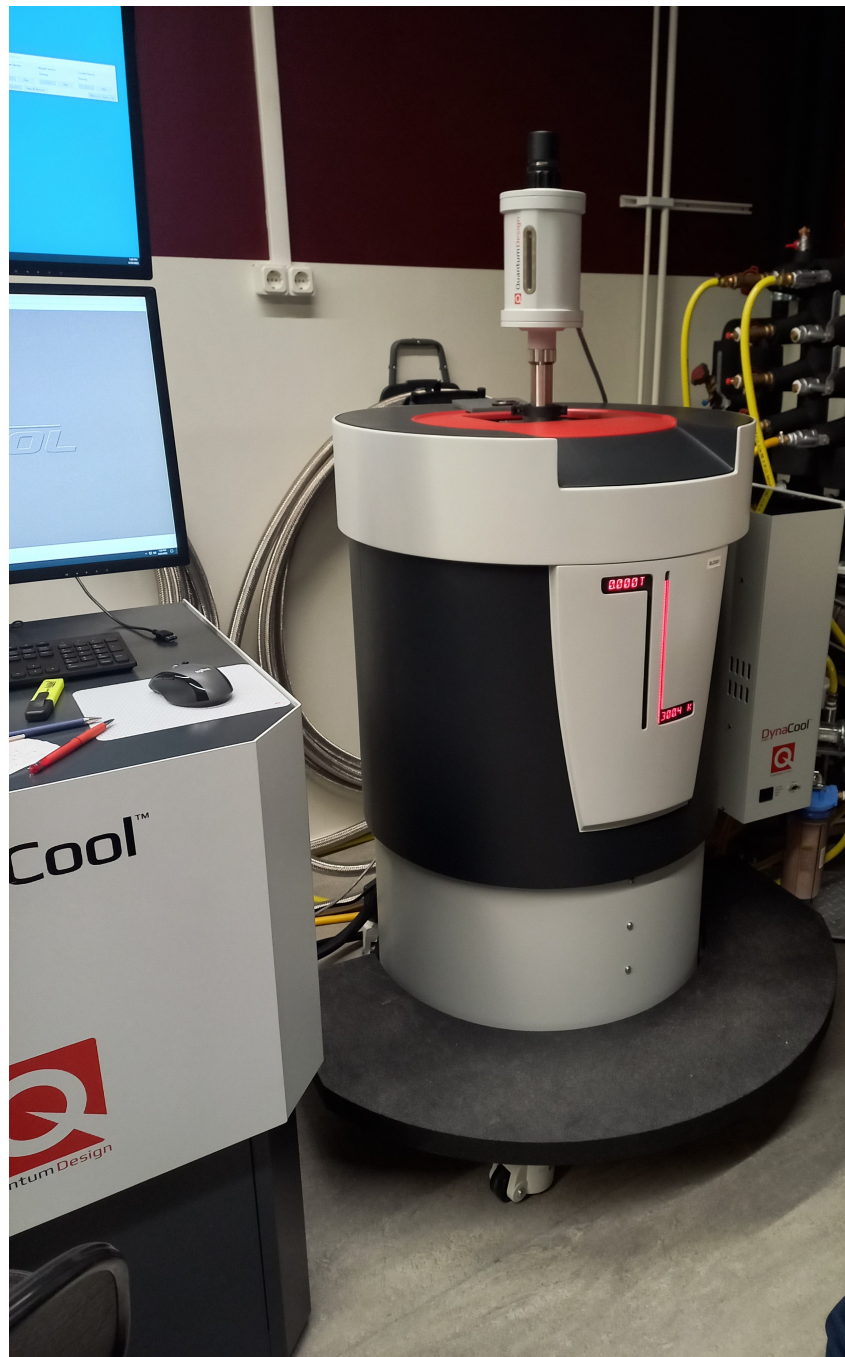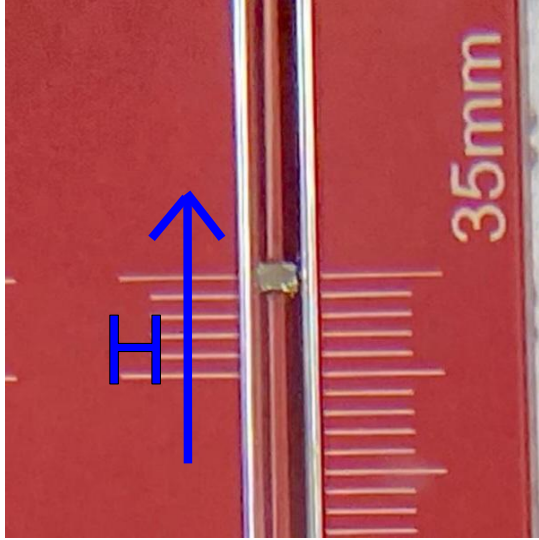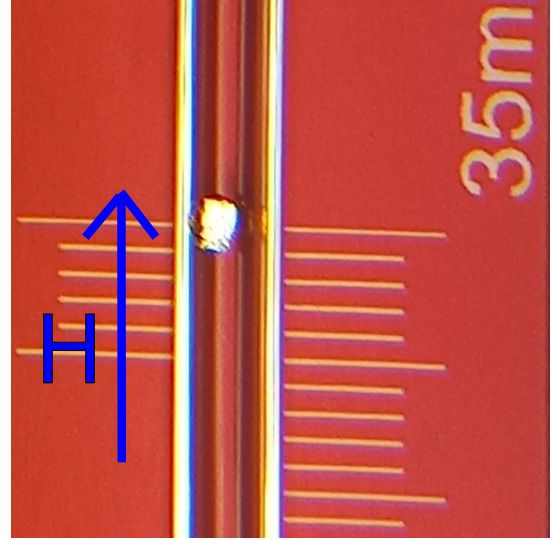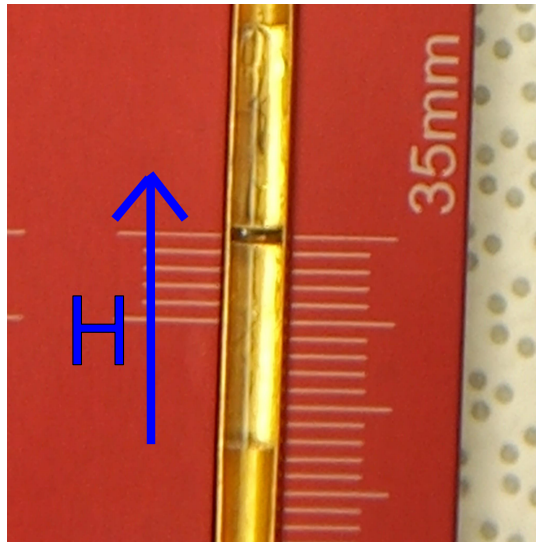
Figure 5: PPMS used for measurements. Made by Quantum Design [15].

(a) First position of sample, with the magnetic field along the a-axis.

(b) Second position of sample, with the magnetic field along the b-axis.

(c) Third position of sample, with the magnetic field along the c-axis.

Figure 6: Sample mounted on holder before each M vs. T experiment. During each experiment, the magnetic field was going from the bottom to the top of the image, as shown by the blue arrows.

100 K, 75 K, 50 K, 20 K and 5 K.

3   Results

3.1   Magnetization vs. Temperature Results

The magnetization measurements for the a-axis of the sample is found in Figure 7a. The magnetization for the b-axis is found in Figure 7b. The magnetization of the c-axis is found in Figure 7c. A comparison between the χ for the a and b axis for each temperature is found in Figure 11. From Figure 7a, we can see that a splitting between ZFC and FC occurs, with the highest difference being 5.03e-6 emu/(cm^{3}Oe)

## 3.2   Magnetization vs. Magnetic Field Results

The M vs. H measurements were only done for the b- and c-axis, resulting in two very different graphs. The graph for M vs. H for the b-axis is found in Figure 9, while the M vs. H graph for the c-axis is found in figure Figure 10.

3.3   Analysis

By analysing the results, further conclusions about the magnetic properties of CrSb may be drawn.

3.3.1   Magnetic Anisotropy

By comparing the susceptibility as a function of temperature between the a- and b-axis, it can be seen that CrSb is anisotropic due to the difference in magnetic susceptibility between different orientations of the material. Specifically, the b-axis shows a larger susceptibility and, unlike the a-axis, no splitting between the ZFC and FC measurements. The difference in susceptibility between the axes can be found in Figure 11. For data compiling the highest, lowest and average difference, see Table 1.
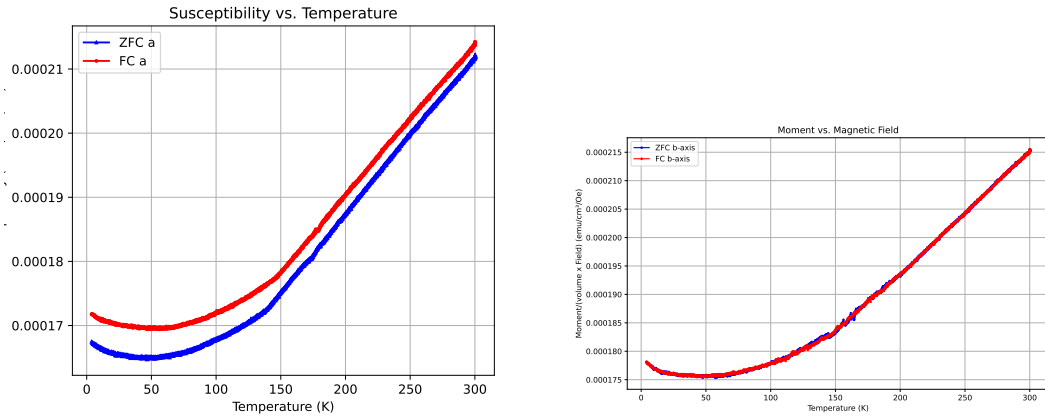
(a) M vs. T for the a-axis. FC-ZFC splitting is observed with FC displaying a higher susceptibility.

(b) M vs. T for the b-axis. No FC-ZFC splitting can be observed as any difference is within the error of measurement.
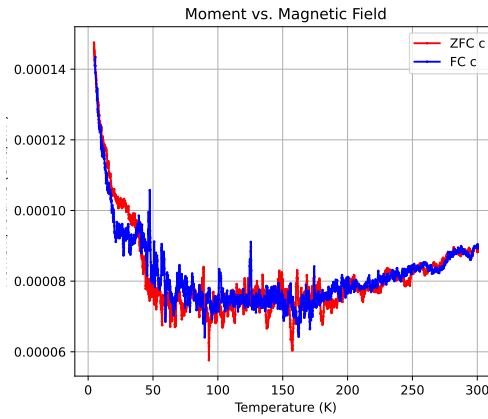
(c) M vs. T for the c-axis. Data very noisy due to thinness of sample in this orientation.

Figure 7: M vs. T measurements for 3 different orientations, denoted a-axis, b-axis and c-axis respectively. The x-axes show the temperature measured in Kelvin, the y-axes the volume susceptibility measured in emu/cm³/Oe.

Table 1: Relevant data over the difference in susceptibility between the a-axis and b-axis.

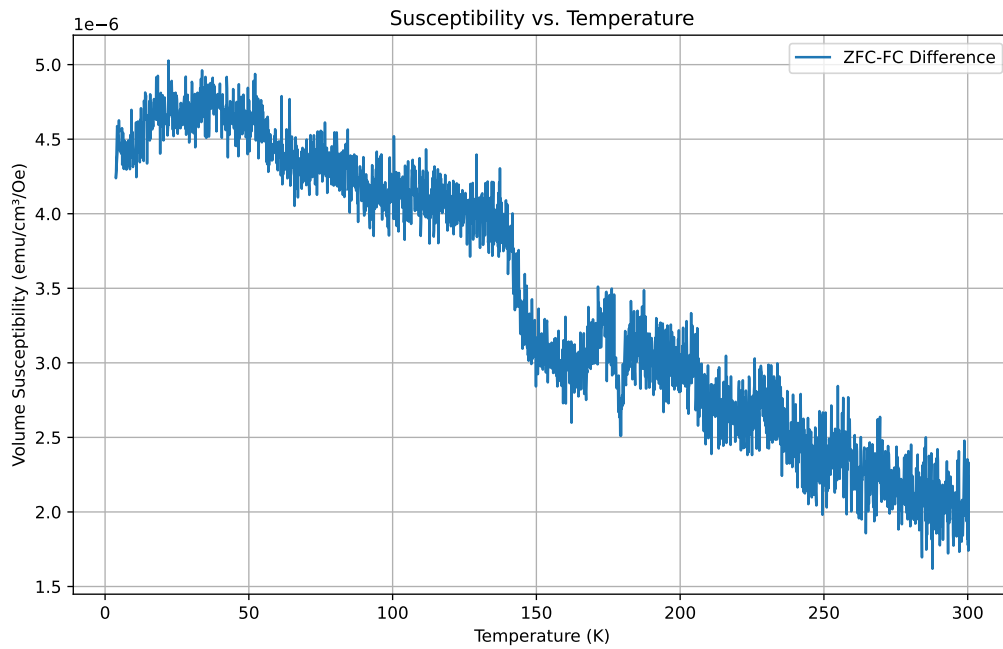| Value	ZFC	FC
Highest Difference	1.109e-05 emu/cm³/Oe	6.637e-06 emu/cm³/Oe
Lowest Difference	3.030e-06 emu/cm³/Oe	8.968e-07 emu/cm³/Oe
Average Difference	7.805e-06 emu/cm³/Oe	4.357e-06 emu/cm³/Oe

Figure 8: Difference in magnetic susceptibility between ZFC and FC for the a-axis. The average difference was found to be around 3.427e-06 emu/cm^3/Oe. The x-axis shows the temperature measured in Kelvin, the y-axis the volume susceptibility measured in emu/cm^3/Oe.

3.3.2   ZFC-FC Splitting

As mentioned, the measurements along the b-axis does not show any ZFC-FC splitting, but the a-axis does. The FC case shows a higher susceptibility. The difference in susceptibility between the ZFC and FC cases for the a-axis is found in Figure 8.

3.3.3   Temperature Dependence

Both the a- and b-axis show an increasing susceptibility with increasing temperature. This does not follow the standard Curie-Weiss behaviour and thus requires us to use a modified version of it which includes a temperature independent term χ_0 and a linear term aT, as described in Equation (10).

By using the python library *Scipy*, a curve with the formula shown in Equation (10) can be fitted and values for C, θ_{CW}, χ_0 and a can be found. However, creating a fit over the entire temperature range yields values for the parameters which are unphysical or a
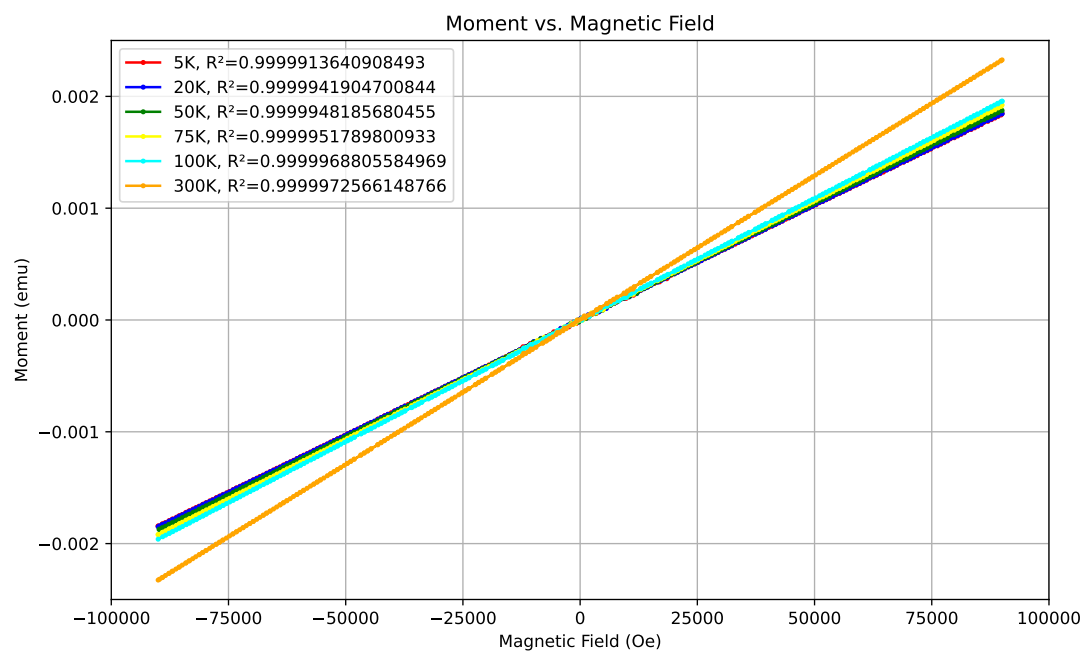
Figure 9: M vs. H measurements for different temperatures along the b-axis. All R²
values for linear fits of the data are 1.000 when using 4 significant figures, meaning the
susceptibility is indeed linearly dependent on the applied field. The x-axis shows the
magnetic field measured in Oe, while the y-axis shows the magnetic moment measured in
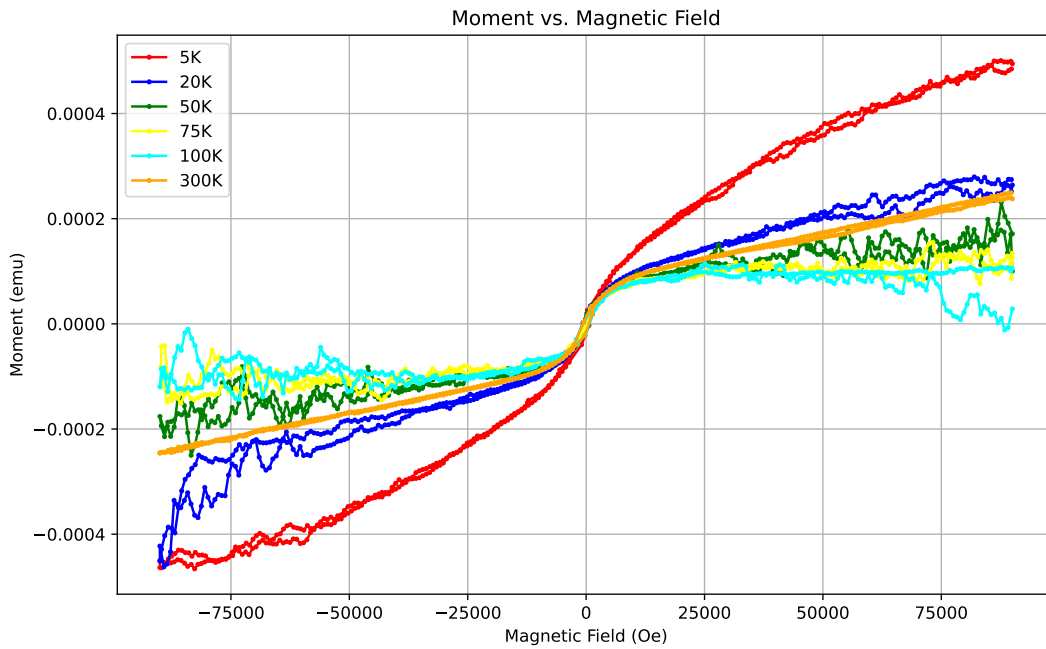emu.

Figure 10: M vs. H measurements for different temperatures along the c-axis. Unlike the b-axis, the magnetic moment was not linearly dependent on the magnetic field. The x-axis shows the magnetic field measured in Oe, while the y-axis shows the magnetic moment measured in emu.

fit which does not fit the data that well. This can be resolved by restraining the fit to only be over a smaller part of the temperature range. The best suited range was found to be around the 50-300 K temperature range, which the fitted line in Figure 12 is based around.

For our purposes, the Curie Constant C is the most interesting. The fitted curve and constant C for the a-axis is found in Figure 12. Using Equation (5), the effective magnetic moment can be found with the help of the Curie Constant, see Table 2. The magnetic moment for Cr^{3+} ions can be calculated from Equation (6) using $n = 3$, which yields a magnetic moment for Cr^{3+} as $\mu_{eff} \approx 3.87\mu_B$.

The c-axis temperature dependence was different from the a-axis and b-axis. In particular, there appears to be a shoulder near the 5-25 K range, displaying a curve which starts with a rapid decrease in magnetization as the temperature increases, before leveling out and seeing an increase in magnetization with the increasing temperature. The c-axis
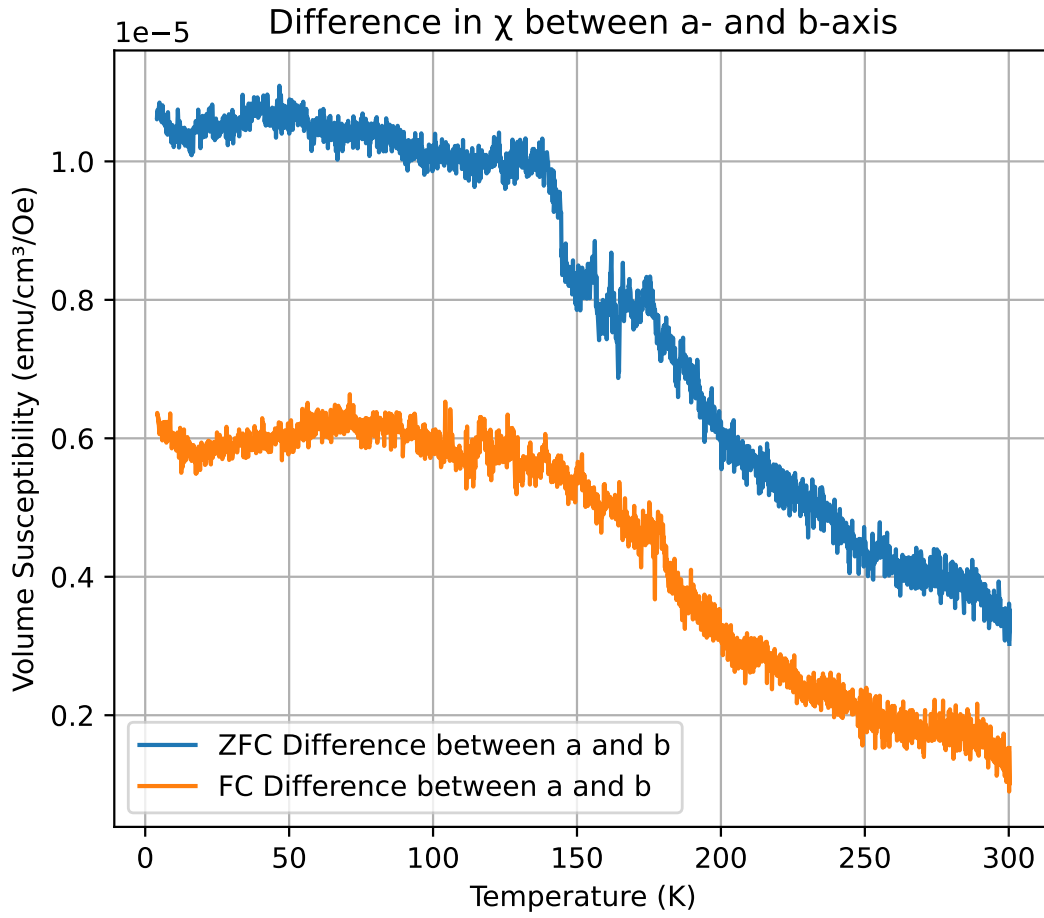
Figure 11: The difference in susceptibility between the two main orientations, the a-axis and the b-axis. Both ZFC and FC differences were calculated. The x-axis shows the temperature measured in Kelvin, the y-axis the volume susceptibility measured in emu/cm³/Oe.
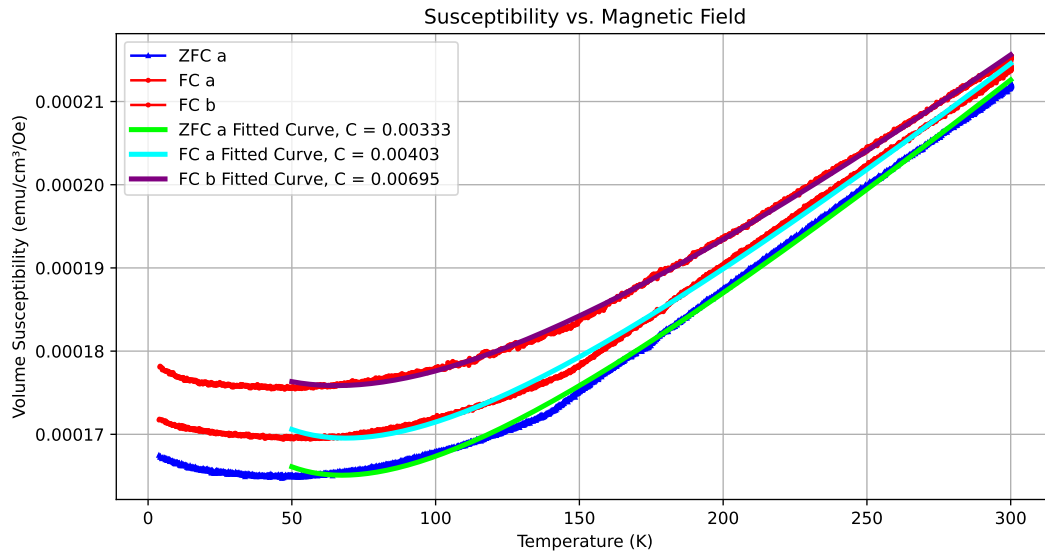
Figure 12: ZFC a-axis, FC a-axis and FC b-axis data plotted together with fitted curves and extracted Curie Constant. The x-axis shows the temperature measured in Kelvin, the y-axis the volume susceptibility measured in emu/cm³/Oe.

Table 2: Extracted Curie Constants and effective magnetic moments measured in Bohr Magnetons. One standard deviation from the fitted data is specified.

Data	Curie Constant	Effective Moment μ_{eff}
ZFC a-axis	0.003329 ± 0.0001481	$0.163\mu_B$
FC a-axis	0.004028 ± 0.0001862	$0.179\mu_B$
FC b-axis	0.00695 ± 0.0002583	$0.236\mu_B$

does nor display any signs of ZFC-FC splitting outside the expected error due to the noise of the data.

3.3.4   Fitted Magnetization vs. Magnetic Field and Hysteresis

The M vs. H graphs plotted in Figure 9 and Figure 10 show that the b-axis and c-axis do not feature any magnetic hysteresis. The plots for all temperatures in the b-axis are completely linear and a fitted linear regression yields a R^2 value of 1.000 after rounding to 4 significant figures. The lack of hysteresis signifies either antiferromagnetic or paramagnetic behaviour. The graph for the c-axis is far more noisy. This is due to how thin the sample was in the c-axis, leading to a smaller registered magnetic moment which means that the noise has a higher impact on the measurements. The lines are noted to not be linear, however, no signs of a hysteresis loop can be seen. How thin the sample is also affects the

contribution of the surface of the sample which, due to not being positioned within the crystal and some atoms missing neighbours, leads to different behaviour.

4   Discussion

The results found within this report can be used to attempt to characterize the nature of CrSb's altermagnetic properties. The magnetic anisotropy has been determined to exist, with the b-axis being the easiest direction for magnetization. The increase in susceptibility along the b-axis was on average around 7.8×10^{-6} emu/cm^3/Oe higher than the susceptibility of the ZFC measurements along the a-axis. The ZFC-FC splitting was observed only in the a-axis where a FC measurement yielded an on average 3.427e-06 emu/cm^3/Oe. The b- and c-axes showed no ZFC-FC splitting greater than the error in the data. The splitting in the a-axis suggest minor freezing effects for the alignment of magnetic moments.

The difference between the calculated effective magnetic moment for Cr^{3+} ions and the one calculated from the extracted Curie Constant shows that there is itinerant magnetism present within CrSb. If the localized moments were the sole contributors to magnetism, the calculated effective moment would be the same as the one found through the measurements. The Moment vs. Magnetic Field graph in Figure 9 is also consistent with what would be expected from a itinerant antiferromagnet. This means that any attempt to further characterize the magnetic properties of CrSb would require other more sophisticated models which can correctly take the interactions between the electrons into account. The Moment vs. Magnetic Field graph for the c-axis, seen in Figure 10, needs to be further studied, as it is nonlinear while simultaneously showing no signs of a hysteresis loop. Performing more measurements with a large sample with more thickness in the c-axis would reduce the noise and surface contributions found within this study.

4.1   Conclusion

From the analysis, one can conclude that CrSb crystals are anisotropic from the difference in susceptibility between the axes. Specifically, the b-axis was shown to be an easy axis, which is useful to know for future applications of CrSb as a altermagnetic material. The temperature dependence did not follow a standard Curie-Weiss law, due to the susceptibility increasing over the entire temperature range, while the standard Curie-Weiss law predicts decreasing susceptibility with increasing temperature. This suggests itinerant magnetism or other magnetic contributions such as Pauli-paramagnetism. Using a modified Curie-Weiss law with a temperature independent term and a linear term gave a better fit when used over the 50-300 K range. CrSb has also been shown to display a ZFC-FC splitting, however only over the a-axis.

4.2   Sources of Error

During measurements of the magnetic susceptibility, there will always be a diamagnetic contribution from the sample holder which, by necessity, will move with the sample through the magnetic field. While the diamagnetic contribution is usually small, the small size of the sample itself means that there is a risk that the diamagnetic contribution can not be ignored.

There is also a risk for a residual magnetic field to be present within the PPMS. During the ZFC measurements, a residual magnetic field could interfere with the measurements and not provide a true picture of how a ZFC CrSb sample would behave. Any residual material from earlier experiments could also contribute to thus unaccounted for magnetic field.

The fitting of the Magnetization vs. Temperature data could also contain sources of error. Due to the unnatural fit when considering the entire temperature range, a smaller range was chosen instead. However, a different range could have had the potential to provide even better values of the Curie constant. The one used should be sufficiently accurate to

use the general results, but for a more exact value for the Curie constant to be extracted, more sophistication in measurements or data analysis needs to be used.

4.3 Outlook

Future studies of CrSb will need to use more sophisticated models than merely band structure theory. A better understanding of the susceptibility of CrSb crystals along the c-axis would be attained if one lessens the contributions of the surface by increasing the width of the sample. A more exact mapping of the a-, b- and c-axes to the crystal structure would also be beneficial as this study merely analyses whether a magnetic anisotropy exist but not along which axes in the crystal structure that the a-, b- and c-axes represent.

References

[1] J. Krempaskỳ, L. Šmejkal, S. D'souza, M. Hajlaoui, G. Springholz, K. Uhlířová, F. Alarab, P. Constantinou, V. Strocov, D. Usanov, *et al.*, "Altermagnetic lifting of kramers spin degeneracy," *Nature*, vol. 626, no. 7999, pp. 517–522, 2024.

[2] L. Šmejkal, J. Sinova, and T. Jungwirth, "Emerging research landscape of altermagnetism," *Physical Review X*, vol. 12, no. 4, p. 040501, 2022.

[3] S. Mugiraneza and A. M. Hallas, "Tutorial: a beginner's guide to interpreting magnetic susceptibility data with the curie-weiss law," *Communications Physics*, vol. 5, no. 1, p. 95, 2022.

[4] L. Bennett, C. Page, and L. Swartzendruber, "Comments on units in magnetism," *JOURNAL OF RESEARCH of the National Bureau of Standards*, vol. 83, no. 1, p. 9, 1978.

[5] C. Kittle, *Introduction to Solid State Physics*. John Wiley & Sons, Inc, 8 ed., 2005.

[6] J. Foadi and G. Evans, "Elucidations on the reciprocal lattice and the ewald sphere," *European Journal of Physics*, vol. 29, p. 1059, aug 2008.

[7] J. Güémez, M. Fiolhais, and L. A. Fernández, "The principle of relativity and the de broglie relation," *American Journal of Physics*, vol. 84, no. 6, pp. 443–447, 2016.

[8] K. Suto, "An energy-momentum relationship for a bound electron inside a hydrogen atom.," *Physics Essays*, vol. 24, no. 2, 2011.

[9] A. Kahn, "Fermi level, work function and vacuum level," *Materials Horizons*, vol. 3, no. 1, pp. 7–10, 2016.

[10] C. Song, H. Bai, Z. Zhou, L. Han, H. Reichlova, J. H. Dil, J. Liu, X. Chen, and F. Pan, "Altermagnets as a new class of functional materials," *Nature Reviews Materials*, pp. 1–13, 2025.

[11] M. V. Berry and A. K. Geim, "Of flying frogs and levitrons," *European Journal of Physics*, vol. 18, no. 4, p. 307, 1997.

[12] R. Tamang, S. Gurung, D. Rai, S. Brahimi, and S. Lounis, "Altermagnetism and altermagnets: A brief review," 2025.

[13] X. Peng, Y. Wang, S. Zhang, Y. Zhou, Y. Sun, Y. Su, C. Wu, T. Zhou, L. Liu, H. Wang, *et al.*, "Scaling behavior of magnetoresistance and hall resistivity in the altermagnet crsb," *Physical Review B*, vol. 111, no. 14, p. 144402, 2025.

[14] G. Yang, Z. Li, S. Yang, J. Li, H. Zheng, W. Zhu, Z. Pan, Y. Xu, S. Cao, W. Zhao, *et al.*, "Three-dimensional mapping and electronic origin of large altermagnetic splitting near fermi level in crsb," *arXiv preprint arXiv:2405.12575*, 2024.

[15] Quantum Design, 6325 Lusk Boulevard San Diego, CA 92121 USA, *Vibrating Sample Magnetometer (VSM) Option User's Manual*, 5 ed., February 2011.